

Synthesis, Characterization, and Photophysical Properties of Os(II) Diimine Complexes $[\text{Os}(\text{N}\wedge\text{N})(\text{CO})_2\text{I}_2]$ ($\text{N}\wedge\text{N}$ = Bipyridine, Phenanthroline, and Pyridyl Benzoxazole)

Yao-Lun Chen, Shih-Wen Lee, Yun Chi,* Kuo-Chu Hwang, and Sujit Baran Kumar

Department of Chemistry, National Tsing Hua University, Hsinchu 30013, Taiwan

Ya-Hui Hu, Yi-Ming Cheng, Pi-Tai Chou,* Shie-Ming Peng, and Gene-Hsiang Lee

Department of Chemistry and Instrumentation Center, National Taiwan University, Taipei 10764, Taiwan

Shi-Jay Yeh and Chin-Ti Chen*

Institute of Chemistry, Academia Sinica, Taipei 11529, Taiwan

Received January 11, 2005

A new series of Os(II) diimine complexes with the general formula $[\text{Os}(\text{N}\wedge\text{N})(\text{CO})_2\text{I}_2]$, $\text{N}\wedge\text{N}$ = 2,2'-bipyridine (bpy) (1), 4,4'-di-*tert*-butyl-2,2'-bipyridine (dbubpy) (2), 4,7-diphenyl-1,10-phenanthroline (dpphen) (3), 2-(2'-pyridyl)-benzoxazole (pboz) (4), and 5-*tert*-butyl-2-(2'-pyridyl)benzoxazole (bupboz) (5), were synthesized and characterized by spectroscopic methods and by a single-crystal X-ray diffraction study on the dpphen complex 3. The corresponding photophysical properties were studied using UV-vis and emission spectrometry. The resulting phosphorescence features both in solution and as a solid film, in combination with the MO calculation, lead us to conclude that the emissions originate from mixed halide-to-ligand (XLCT ~70%) and metal-to-ligand (MLCT ~30%) transitions instead of the typical MLCT transition. Using complexes 4 and 5 as the dopant emitters, we evaluated their potential to serve as a phosphor for organic light emitting diodes by examining their electroluminescent performances. Reddish orange electroluminescence centered around 600 nm was observed for organic light emitting diodes (OLEDs) fabricated using complex 5 as the emitter; the device efficiency was shown to be as high as 2.8% (and 5.0 cd/A or 2.7 lm/W), and the peak luminance was shown to be 5600 cd/m² at a driving voltage of ~15 V.

1. Introduction

The synthesis and characterization of light emitting diimine transition metal complexes continue to attract much attention mainly because of their potential in various technical applications, such as chemical sensors,¹ sensitizers in solar energy conversion,² and emitting materials for organic light emitting diodes (OLEDs).³ Thus, it becomes important to shed light on the nature and dynamics of their excited states.

A particularly important class of these complexes is the Re(I) carbonyl complexes *fac*-[Re(N \wedge N)(CO)₃X], in which the chelating diimine, N \wedge N, is a bidentate heterocycle such as 2,2'-bipyridine, 1,10-phenanthroline, or their substitutional derivatives,⁴ while the monodentate ligand, X, can be halides, pseudo halides, or even more complicated organic ligands such as pyridine or acetylide.⁵ As expected, most of these Re(I) complexes are known to exhibit strong emission in

* To whom correspondence should be addressed. E-mail: ychi@mx.nthu.edu.tw. Fax: (886) 3572-0864 (Y.C.). E-mail: chop@ntu.edu.tw. Fax: (886) 2 2363-6539 (P.-T.C.). E-mail: cchen@chem.sinica.edu.tw. Fax: (886) 2 2783-1237 (C.-T.C.).

(1) (a) Shen, Y.; Sullivan, B. P. *J. Chem. Educ.* **1997**, *74*, 685. (b) Sun, S.-S.; Lees, A. J. *Organometallics* **2002**, *21*, 39. (c) Demas, J. N.; DeGraff, B. A. *Coord. Chem. Rev.* **2001**, *211*, 317. (d) Vogler, A.; Kunkely, H. *Top. Curr. Chem.* **2001**, *213*, 143.

- (2) (a) Hagfeldt, A.; Gratzel, M. *Acc. Chem. Res.* **2000**, *33*, 269. (b) Balzani, V.; Juris, A. *Coord. Chem. Rev.* **2001**, *211*, 97. (c) Paw, W.; Cummings, S. D.; Mansour, M. A.; Connick, W. B.; Geiger, D. K.; Eisenberg, R. *Coord. Chem. Rev.* **1998**, *171*, 125.
- (3) (a) Carlson, B.; Phelan, G. D.; Kaminsky, W.; Dalton, L.; Jiang, X. Z.; Liu, S.; Jen, A. K.-Y. *J. Am. Chem. Soc.* **2002**, *124*, 14162. (b) Gao, F. G.; Bard, A. J. *J. Am. Chem. Soc.* **2000**, *122*, 7426. (c) Baldo, M. A.; O'Brien, D. F.; You, Y.; Shoustikov, A.; Sibley, S.; Thompson, M. E.; Forrest, S. R. *Nature* **1998**, *395*, 151.

degassed fluid solutions at room temperature, and their photophysical properties can be tailored by systematically varying the diimine chromophore and the anionic ancillary ligand X. The electronic transition responsible for the luminescence in these Re(I) complexes was derived from the states that involve the ligand-centered $^3\pi\pi^*$ characters, the metal-to-ligand charge transfer ($^3\text{MLCT}$),⁶ or the halide-to-ligand charge-transfer (XLCT) transition,⁷ for which the nature of the lowest-energy excited state is critically dependent on the ancillary ligand associated with the complexes. The high MLCT emission efficiency has stimulated the studies using rhodium-based carbonyl complexes as dopant emitters for fabrication of electrophosphorescent OLEDs.⁸

Likewise, investigations of isoelectronic group 6 analogues, such as $[\text{Ru}(\text{N}\wedge\text{N})(\text{CO})_2\text{X}_2]$,⁹ were conducted. Again, variation of the diimine ligand, N \wedge N, and the ancillary ligands, X, caused dramatic and systematic changes of the character of the lowest excited state with a concomitant strong effect on their chemical properties.^{7,10} However, in this Ru system both the ligand-to-metal bond strength and the heavy atom-induced spin–orbit coupling are notably reduced in comparison with those of their third-row metal counterparts. Ultimately, these properties led to a reduced thermal stability and poor phosphorescent efficiency measured at room temperature which makes them less desirable for the OLED applications.

In this article, we wish to report the synthesis, characterization, and photophysical behavior of the closely related, but more robust, third-row metal analogues (i.e., the Os(II) diimine complexes with the formula $[\text{Os}(\text{N}\wedge\text{N})(\text{CO})_2\text{I}_2]$, in which N \wedge N = 2,2'-bipyridine (bpy) (**1**), 4,4'-di-*tert*-butyl-

2,2'-bipyridine (dbubpy) (**2**), 4,7-diphenyl-1,10-phenanthroline (dpphen) (**3**), 2-(2'-pyridyl)benzoxazole (pboz) (**4**), and 5-*tert*-butyl-2-(2'-pyridyl)benzoxazole (bupboz) (**5**)). In addition, the electroluminescence (EL) properties of complexes **4** and **5** were explored, and orange color emitting devices were fabricated using these Os complexes as the dopant emitter configured at a typical multilayer architecture.

2. Experimental Section

General Information and Materials. All of the solvents were dried before use. Osmium dimer complex $[\text{Os}(\text{CO})_3\text{I}_2]_2$ was synthesized via the reaction of $\text{Os}_3(\text{CO})_{12}$ with 3 equiv of iodine in a stainless autoclave according to a literature procedure (180 °C, 18 h).¹¹ Diimine ligands such as 2,2'-bipyridine (bpy), 4,7-diphenyl-1,10-phenanthroline (dpphen), and 4,4'-di-*tert*-butyl-2,2'-bipyridine (dbubpy) were purchased from commercial suppliers and used without purification, while 2-(2'-pyridyl)benzoxazole (pboz) and 5-*tert*-butyl-2-(2'-pyridyl)benzoxazole (bupboz) were prepared using a previously reported procedure.¹² All of the synthetic manipulations were monitored by TLC with Merck precoated glass plates (0.20 mm with fluorescent indicator UV₂₅₄). Compounds were visualized with UV light irradiation at 254 and 365 nm. Column chromatography was carried out using silica gel from Merck (230–400 mesh). Mass spectra were obtained on a JEOL SX-102A instrument operating in electron impact (EI) mode. IR spectra were recorded on a Perkin-Elmer 2000 FT-IR spectrometer. Both the ¹H and ¹³C NMR spectra were recorded on Varian Mercury-400 or INOVA-500 instruments; chemical shifts are reported with respect to the internal standard, Me₄Si.

Measurement Techniques. Cyclic voltammetry (CV) measurements were performed using a CHI 611A electrochemical analyzer (CH Instrument). The oxidation and reduction measurements were recorded in anhydrous CH_2Cl_2 and THF containing 0.1 M (NBu)₄PF₆ as the supporting electrolyte, respectively, at a scan rate of 100 mV s⁻¹. The potentials were measured against an Ag/Ag⁺ (0.01 M AgNO_3) reference electrode with ferrocene as the internal standard.

Steady-state absorption and emission spectra were recorded by a Hitachi (U-3310) spectrophotometer and an Edinburgh (FS920) fluorimeter, respectively. Both the wavelength-dependent excitation and emission responses of the fluorimeter were calibrated. A configuration of the front-face excitation was used to measure the emission of the solid sample, for which the cell was made by assembling two edge-polished quartz plates with various Teflon spacers. A combination of appropriate filters was used to avoid interference from the scattering light. The methods for the quantum-yield measurements for complexes **1**–**5** in either solution or solid film have been elaborated in our previous paper.¹³

Lifetime studies were performed with an Edinburgh FL 900 photon-counting system with a hydrogen-filled or nitrogen lamp as the excitation source. Data were analyzed using the nonlinear least-squares procedure in combination with an iterative convolution method. The emission decays were analyzed by the sum of the

- (4) (a) Stufkens, D. J. *Comments Inorg. Chem.* **1992**, *13*, 359. (b) Wang, Y.; Hauser, B. T.; Rooney, M. M.; Burton, R. D.; Schanze, K. S. *J. Am. Chem. Soc.* **1993**, *115*, 5675. (c) Guerrero, J.; Piro, O. E.; Wolkan, E.; Feliz, M. R.; Ferraudi, G.; Moya, S. A. *Organometallics* **2001**, *20*, 2842. (d) Lo, K. K.-W.; Hui, W.-K.; Ng, D. C.-M.; Cheung, K.-K. *Inorg. Chem.* **2002**, *41*, 40.
- (5) (a) Zipp, A. P.; Sacksteder, L.; Streich, J.; Cook, A.; Demas, J. N.; DeGraff, B. A. *Inorg. Chem.* **1993**, *32*, 5629. (b) Yam, V. W.-W. *Chem. Commun.* **2001**, 789. (c) Yam, V. W.-W. *Acc. Chem. Res.* **2002**, *35*, 555.
- (6) (a) Sacksteder, L.; Zipp, A. P.; Brown, E. A.; Streich, J.; Demas, J. N.; DeGraff, B. A. *Inorg. Chem.* **1990**, *29*, 4335. (b) Walters, K. A.; Premvardhan, L. L.; Liu, Y.; Peteau, L. A.; Schanze, K. S. *Chem. Phys. Lett.* **2001**, *339*, 255. (c) Striplin, D. R.; Crosby, G. A. *Coord. Chem. Rev.* **2001**, *211*, 163.
- (7) (a) Nieuwenhuis, H. A.; Stufkens, D. J.; Vlcek, A., Jr. *Inorg. Chem.* **1995**, *34*, 3879. (b) van Slageren, J.; Hartl, F.; Stufkens, D. J.; Martino, D. M.; Van Willigen, H. *Coord. Chem. Rev.* **2000**, *208*, 309.
- (8) (a) Gong, X.; Ng, P. K.; Chan, W. K. *Adv. Mater.* **1998**, *10*, 1337. (b) Li, Y.; Wang, Y.; Zhang, Y.; Wu, Y.; Shen, J. *Synth. Met.* **1999**, *99*, 257. (c) Chan, W. K.; Ng, P. K.; Gong, X.; Hou, S. *Appl. Phys. Lett.* **1999**, *75*, 3920. (d) Li, Y.; Liu, Y.; Guo, J.; Wu, F.; Tian, W.; Li, B.; Wang, Y. *Synth. Met.* **2001**, *118*, 175. (e) Wang, K.; Huang, L.; Gao, L.; Jin, L.; Huang, C. *Inorg. Chem.* **2002**, *41*, 3353. (f) Ranjan, S.; Lin, S.-Y.; Hwang, K.-C.; Chi, Y.; Ching, W.-L.; Liu, C.-S.; Tao, Y.-T.; Chien, C.-H.; Peng, S.-M.; Lee, G.-H. *Inorg. Chem.* **2003**, *42*, 1248.
- (9) (a) Kleverlaan, C. J.; Stufkens, D. J.; Fraanje, J.; Goubitz, K. *Eur. J. Inorg. Chem.* **1998**, 1243. (b) Rossenaar, B. D.; Stufkens, D. J.; Vlcek, A., Jr. *Inorg. Chem.* **1996**, *35*, 2902. (c) van Slageren, J.; Stufkens, D. J. *Inorg. Chem.* **2001**, *40*, 277.
- (10) (a) Aartsen, M. P.; Stufkens, D. J.; Wilms, M. P.; Baerends, E. J.; Vlcek, A., Jr.; Clark, I. P.; George, M. W.; Turner, J. J. *Chem.—Eur. J.* **1996**, *2*, 1556. (b) Stufkens, D. J.; Vlcek, A., Jr. *Coord. Chem. Rev.* **1998**, *177*, 127.
- (11) Moss, J. R.; Niven, M. L.; Sutton, E. E. *Inorg. Chim. Acta* **1988**, *147*, 251.
- (12) Yoshifumi, M.; Nagase, R.; Kawashima, T.; Inamoto, N. *Heterocycles* **1978**, *10*, 57.
- (13) (a) Yu, J.-K.; Hu, Y.-H.; Cheng, Y.-M.; Chou, P.-T.; Peng, S.-M.; Lee, G.-H.; Carty, A. J.; Tung, Y.-L.; Lee, S.-W.; Chi, Y.; Liu, C.-S. *Chem.—Eur. J.* **2004**, *10*, 6255. (b) Chen, H.-Y.; Chi, Y.; Liu, C.-S.; Yu, J.-K.; Chen, K.-S.; Chou, P.-T.; Peng, S.-M.; Lee, G.-H.; Carty, A. J.; Yeh, S.-J.; Chen, C.-T. *Adv. Funct. Mater.* **2005**, *15*, 567.

exponential functions which allows partial removal of the instrument time broadening and consequently renders a temporal resolution of ~ 200 ps.

Computational Methodology. Calculations on the electronic ground states of complexes **1–5** were carried out using B3LYP density functional theory.^{14,15} Double- ζ quality basis sets were employed for the ligands, 6-31G*, and the iodide and osmium atoms, LANL2DZ. A relativistic effective core potential (ECP) on osmium¹⁶ replaced the inner core electrons leaving the outer core (5s²5p⁶) electrons and the 5d⁶ valence electrons of Os(II) metal ion. A time-dependent DFT (TDDFT) calculation¹⁷ using the B3LYP functional was then performed on the basis of the optimized geometry to analyze the excited-state energetics and the associated frontier orbitals. Typically, the lowest 10 triplet and 10 singlet roots of the nonhermitian eigenvalue equations were obtained to determine the vertical excitation energies. Oscillator strengths were deduced from the dipole transition matrix elements (for singlet states only). The ground-state B3LYP and excited-state TDDFT calculations were carried out using Gaussian 03.¹⁸ The percentage compositions of the molecular orbitals were calculated using the AOMix program.¹⁹

Synthesis of 1. Finely pulverized [Os(CO)₃I₂]₂ (300 mg, 0.28 mmol) and 2,2'-bipyridine (100 mg, 0.64 mmol) were thoroughly mixed and loaded into a 10 mL Carius tube. The tube was sealed under a vacuum and placed into an oven maintained at 160 °C for 2 h. Then, the tube was cooled to room temperature and opened; the contents were extracted into CH₂Cl₂, and the resulting solution was passed through a silica gel column to remove insoluble impurities. The crude product was crystallized from CH₂Cl₂ to yield a yellow crystalline solid of [Os(bpy)(CO)₂I₂] (200 mg, 0.31 mmol, 55%).

Spectral data of **1**. MS (EI, ¹⁹²Os): *m/z* 658 (M⁺), 630 (M – CO)⁺, 602 (M – 2CO)⁺. IR (CH₂Cl₂): ν (CO) 2038 (vs), 1974 (vs) cm⁻¹. ¹H NMR (400 MHz, CDCl₃, 298 K): δ 9.09 (d, ³J_{HH} = 4.8 Hz, 2H), 8.22 (d, ³J_{HH} = 8.0 Hz, 2H), 8.05 (t, ³J_{HH} = 8.0 Hz, 2H), 7.58 (t, ³J_{HH} = 6.0 Hz, 2H). ¹³C NMR (125 MHz, CDCl₃, 298 K): δ 178.0 (2C, CO), 155.2 (2C, C), 153.3 (2C, CH), 139.3 (2C, CH), 127.6 (2C, CH), 123.5 (2C, CH). Anal. Calcd for C₂₀H₂₄N₂O₂I₂·Os: C, 31.26; H, 3.15; N, 3.65. Found: C, 31.31; H, 3.38; N, 3.80.

- (14) Lee, C.; Yang, W.; Parr, R. G. *Phys. Rev. B* **1988**, *37*, 785.
 (15) Becke, A. D. *J. Chem. Phys.* **1993**, *98*, 5648.
 (16) Hay, P. J.; Wadt, W. R. *J. Chem. Phys.* **1985**, *82*, 299.
 (17) (a) Jamorski, C.; Casida, M. E.; Salahub, D. R. *J. Chem. Phys.* **1996**, *104*, 5134. (b) Petersilka, M.; Grossmann, U. J.; Gross, E. K. U. *Phys. Rev. Lett.* **1996**, *76*, 1212. (c) Bauernschmitt, R.; Ahlrichs, R.; Henrich, F. H.; Kappes, M. M. *J. Am. Chem. Soc.* **1998**, *120*, 5052. (d) Casida, M. E. *J. Chem. Phys.* **1998**, *108*, 4439. (e) Stratmann, R. E.; Scuseria, G. E.; Frisch, M. J. *J. Chem. Phys.* **1998**, *109*, 8218.
 (18) Frisch, M. J.; Trucks, G. W.; Schlegel, H. B.; Scuseria, G. E.; Robb, M. A.; Cheeseman, J. R.; Montgomery, J. A., Jr.; Vreven, T.; Kudin, K. N.; Burant, J. C.; Millam, J. M.; Iyengar, S. S.; Tomasi, J.; Barone, V.; Mennucci, B.; Cossi, M.; Scalmani, G.; Rega, N.; Petersson, G. A.; Nakatsuji, H.; Hada, M.; Ehara, M.; Toyota, K.; Fukuda, R.; Hasegawa, J.; Ishida, M.; Nakajima, T.; Honda, Y.; Kitao, O.; Nakai, H.; Klene, M.; Li, X.; Knox, J. E.; Hratchian, H. P.; Cross, J. B.; Bakken, V.; Adamo, C.; Jaramillo, J.; Gomperts, R.; Stratmann, R. E.; Yazyev, O.; Austin, A. J.; Cammi, R.; Pomelli, C.; Ochterski, J. W.; Ayala, P. Y.; Morokuma, K.; Voth, G. A.; Salvador, P.; Dannenberg, J. J.; Zakrzewski, V. G.; Dapprich, S.; Daniels, A. D.; Strain, M. C.; Farkas, O.; Malick, D. K.; Rabuck, A. D.; Raghavachari, K.; Foresman, J. B.; Ortiz, J. V.; Cui, Q.; Baboul, A. G.; Clifford, S.; Cioslowski, J.; Stefanov, B. B.; Liu, G.; Liashenko, A.; Piskorz, P.; Komaromi, I.; Martin, R. L.; Fox, D. J.; Keith, T.; Al-Laham, M. A.; Peng, C. Y.; Nanayakkara, A.; Challacombe, M.; Gill, P. M. W.; Johnson, B.; Chen, W.; Wong, M. W.; Gonzalez, C.; Pople, J. A. *Gaussian 03*, revision C.02; Gaussian, Inc.: Wallingford, CT, 2004.
 (19) (a) Gorelsky, S. I. *AOMix*, revision 6.02, <http://www.sg-chem.net/>. (b) Gorelsky, S. I.; Lever, A. B. P. *Organomet. Chem.* **2001**, *635*, 187.

C₁₂H₈N₂O₂I₂Os: C, 21.94; H, 1.22; N, 4.27. Found: C, 22.19; H, 1.41; N, 4.30.

Synthesis of 2. Finely pulverized [Os(CO)₃I₂]₂ (300 mg, 0.28 mmol) and 4,4'-di-*tert*-butyl-2,2'-bipyridine (dbubpy) (170 mg, 0.64 mmol) were thoroughly mixed and loaded into a 10 mL Carius tube. The tube was sealed under a vacuum and placed into an oven maintained at 200 °C for 6 h. Then, the tube was opened; the contents were extracted into CH₂Cl₂, and the resulting solution was passed through a silica gel column to remove minor products. Further purification by recrystallization from a mixture of CH₂Cl₂ and MeOH yielded 240 mg of yellow crystals of [Os(dbubpy)-(CO)₂I₂] (0.31 mmol, 68%).

Spectral data of **2**. MS (FAB, ¹⁹²Os): *m/z* 770 (M⁺). IR (CH₂Cl₂): ν (CO) 2035 (vs), 1971 (vs) cm⁻¹. ¹H NMR (400 MHz, CDCl₃, 298 K): δ 8.92 (d, ³J_{HH} = 6.0 Hz, 2H), 8.09 (d, ⁴J_{HH} = 1.6 Hz, 2H), 7.53 (dd, ³J_{HH} = 5.8 Hz, ⁴J_{HH} = 1.6 Hz, 2H), 1.45 (s, 18H). ¹³C NMR (125 MHz, CDCl₃, 298 K): δ 178.4 (2C, CO), 164.1 (2C, C), 155.1 (2C, C), 152.6 (2C, CH), 125.0 (2C, CH), 120.1 (2C, CH), 35.6 (2C, C), 30.3 (6C, Me). Anal. Calcd for C₂₀H₂₄N₂O₂I₂·Os: C, 31.26; H, 3.15; N, 3.65. Found: C, 31.31; H, 3.38; N, 3.80.

Synthesis of 3. Finely pulverized [Os(CO)₃I₂]₂ (300 mg, 0.28 mmol) and 4,7-diphenyl-1,10-phenanthroline (dpphen) (210 mg, 0.64 mmol) were thoroughly mixed and loaded into a 10 mL Carius tube. The tube was sealed under a vacuum and placed into an oven maintained at 210 °C for 30 min. After the tube was cooled to room temperature, it was opened, and the contents were subjected to silica gel column chromatography using CH₂Cl₂ as the eluent. Finally, the crude product was crystallized from a CH₂Cl₂ solution to yield an orange crystalline solid of [Os(dpphen)(CO)₂I₂] (150 mg, 18 mmol, 33%).

Spectral data of **3**. MS (EI, ¹⁹²Os): *m/z* 832 (M⁺), 804 (M – CO)⁺, 776 (M – 2CO)⁺. IR (CH₂Cl₂): ν (CO) 2037 (vs), 1973 (vs) cm⁻¹. ¹H NMR (400 MHz, CDCl₃, 298 K): δ 9.43 (d, ³J_{HH} = 5.2 Hz, 2H), 8.08 (s, 2H), 7.82 (d, ³J_{HH} = 5.2 Hz, 2H), 7.55–7.61 (m, 10H, Ph). ¹³C NMR (125 MHz, CDCl₃, 298 K): δ 178.2 (2C, CO), 152.4 (2C, CH), 151.5 (2C, CN), 147.1 (2C, C), 135.1 (2C, *i*-C₆H₅), 130.1 (2C, *p*-C₆H₅), 129.8 (2C, *o*, *m*-C₆H₅), 129.4 (2C, C), 129.3 (2C, *m*, *o*-C₆H₅), 126.3 (2C, CH), 126.0 (2C, CH). Anal. Calcd for C₂₂H₁₆N₂O₂I₂Os: C, 37.49; H, 1.92; N, 3.36. Found: C, 37.74; H, 2.23; N, 3.36.

Synthesis of 4. Finely pulverized [Os(CO)₃I₂]₂ (300 mg, 0.28 mmol) and 2-(2'-pyridyl)benzoxazole (pboz) (130 mg, 0.64 mmol) were thoroughly mixed and loaded into a 10 mL Carius tube. The tube was sealed under a vacuum and placed into an oven maintained at 160 °C for 5 h. After the reaction was completed, the tube was opened; the contents were extracted into CH₂Cl₂, and the resulting solution was passed through a silica gel column to remove minor impurities. The product was crystallized from a saturated solution of CH₂Cl₂ to yield red-orange [Os(pboz)(CO)₂I₂] (230 mg, 0.34 mmol, 60%).

Spectral data of **4**. MS (EI, ¹⁹²Os): *m/z* 697 (M⁺). IR (CH₂Cl₂): ν (CO) 2041 (vs), 1978 (vs) cm⁻¹. ¹H NMR (400 MHz, CDCl₃, 298 K): δ 9.15 (d, ³J_{HH} = 6.0 Hz, 1H), 8.35 (d, ³J_{HH} = 8.0 Hz, 1H), 8.15 (td, ³J_{HH} = 7.2, ⁴J_{HH} = 1.6 Hz, 1H), 8.02 (dd, ³J_{HH} = 7.8, ⁴J_{HH} = 2.0 Hz, 1H), 7.79 (dd, ³J_{HH} = 8.0, ⁴J_{HH} = 2.0 Hz, 1H), 7.73–7.68 (m, 3H). ¹³C NMR (125 MHz, CDCl₃, 298 K): δ 177.3 (1C, CO), 176.5 (1C, CO), 154.5 (1C, CH), 154.1 (1C, C), 150.5 (1C, C), 143.2 (1C, C), 139.7 (1C, CH), 137.8 (1C, C), 129.4 (1C, CH), 129.2 (1C, CH), 128.1 (1C, CH), 125.3 (1C, CH), 119.5 (1C, CH), 112.5 (1C, CH). Anal. Calcd for C₁₄H₈N₂O₃I₂Os: C, 24.15; H, 1.16; N, 4.02. Found: C, 24.46; H, 1.45; N, 4.04.

Synthesis of 5. Finely pulverized [Os(CO)₃I₂]₂ (300 mg, 0.28 mmol) and 5-*tert*-butyl-2-(2'-pyridyl)benzoxazole (bupboz) (165

Table 1. X-ray Structural Data for Complex **3**

C ₂₆ H ₁₆ I ₂ N ₂ O ₂ Os	mol wt = 832.41
monoclinic, <i>P</i> 2 ₁ / <i>n</i>	temp = 295(2) K
<i>a</i> = 7.3613(3) Å	<i>b</i> = 19.6365(9) Å
<i>c</i> = 16.9027(7) Å	β = 93.313(1)°
vol = 2439.2(2) Å ³	<i>Z</i> = 4
<i>D</i> _c = 2.267 g/cm ³	<i>F</i> (000) = 1536
μ (Mo K α) mm ⁻¹	7.785
cryst size	0.32 × 0.06 × 0.04 mm
<i>h</i> , <i>k</i> , <i>l</i> ranges	-9 to 9, -25 to 25, -21 to 20
transmission max, min	0.7459, 0.1896
data/restraints/parameters	5603/0/298
GOF on <i>F</i> ²	1.181
<i>R</i> ₁ , <i>R</i> ₂ with <i>I</i> > 2σ(<i>I</i>)	0.0522, 0.1006
D-map max/min	1.187/-1.540 e/Å ⁻³

Table 2. Selected Bond Distances (Å) and Angles (deg) for Complex **3**

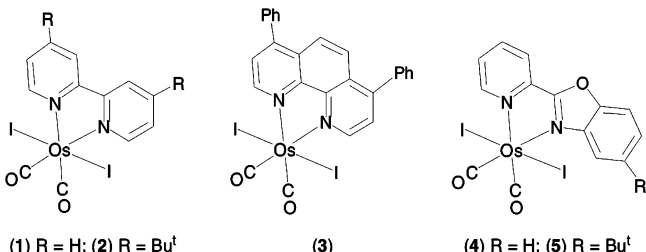
Os—C(1)	1.883(11)	Os—C(2)	1.875(9)
Os—N(1)	2.113(7)	Os—N(2)	2.115(7)
Os—I(1)	2.7002(7)	Os—I(2)	2.6781(7)
O(1)—C(1)	1.110(11)	O(2)—C(2)	1.140(10)
C(1)—Os—C(2)	89.8(4)	N(1)—Os—N(2)	76.5(3)
C(1)—Os—N(2)	172.8(3)	C(2)—Os—N(1)	173.2(3)
I(1)—Os—I(2)	173.93(3)		

mg, 0.64 mmol) were thoroughly mixed and loaded into a 10 mL Carius tube. The tube was sealed under a vacuum and placed into an oven maintained at 180 °C for 5 h. Then, the tube was opened; the contents were extracted into CH₂Cl₂, and the resulting solution was passed through a silica gel column to remove insoluble components. Purification by recrystallization from CH₂Cl₂ and MeOH yielded 295 mg of red [Os(bupboz)(CO)₂I₂] (0.39 mmol, 70%) as a crystalline material.

Spectral data of **5**. MS (FAB, ¹⁹²Os): *m/z* 754 (M⁺). IR (CH₂Cl₂): ν (CO) 2040 (vs), 1977 (vs) cm⁻¹. ¹H NMR (400 MHz, CDCl₃, 298 K): δ 9.12 (d, ³J_{HH} = 5.6 Hz, 1H), 8.31 (d, ³J_{HH} = 8.0 Hz, 1H), 8.15 (t, ³J_{HH} = 8.0 Hz, 1H), 7.96 (s, 1H), 7.76–7.66 (m, 3H), 1.43 (s, 9H). ¹³C NMR (125 MHz, CDCl₃, 298 K): δ 177.4 (1C, CO), 176.9 (1C, CO), 164.2 (1C, C), 154.4 (1C, CH), 152.4 (1C, C), 148.5 (1C, C), 143.2 (1C, C), 139.7 (1C, CH), 137.7 (1C, C), 128.8 (1C, CH), 127.7 (1C, CH), 125.0 (1C, CH), 115.2 (1C, CH), 111.7 (1C, CH), 35.4 (1C, C), 31.4 (3C, Me). Anal. Calcd for C₁₈H₁₆N₂O₃I₂Os: C, 28.73; H, 2.14; N, 3.72. Found: C, 28.97; H, 2.37; N, 3.82.

X-ray Crystallography Analysis. Single-crystal X-ray analysis was performed on a Bruker SMART Apex CCD diffractometer using λ(Mo Kα) radiation (λ = 0.71073 Å). The data collection was executed using the SMART program. Cell refinements and data reduction were made by the SAINT program. The structure was determined using the SHELXTL/PC program and refined using full-matrix least squares. All non-hydrogen atoms were refined anisotropically, whereas the hydrogen atoms were placed at the calculated positions and included in the final stage of refinements with fixed thermal and positional parameters. The crystallographic refinement parameters for complex **3** are summarized in Table 1, and the selected bond distances and angles are listed in Table 2.

Fabrication and Characterization of OLED Devices. The fabrication of OLEDs was conducted via high-vacuum (10⁻⁶ Torr) thermal evaporation of materials onto precleaned indium tin oxide (ITO)-coated glass (Merck Display Technology, Taiwan) with a sheet resistance of less than 50 Ω/sq. The pretreatment of the ITO glass includes a routine chemical cleaning using detergent and alcohol in sequence, followed by an oxy-plasma cleaning. The measurements for the device were made at room temperature under

Scheme 1(1) R = H; (2) R = Bu^t

(3)

(4) R = H; (5) R = Bu^t

ambient conditions. The electroluminescence characterization of the devices has been described elsewhere.²⁰

3. Results

Preparation and Characterization. Diimine osmium complexes **1–5** were synthesized in good yields from the osmium carbonyl compound [Os(CO)₃I₂] and the respective diimine ligand via direct thermolysis of the powdery reactants in the absence of organic solvent. The molecular drawings of relevant Os metal complexes are depicted in Scheme 1. For each experiment, the reactants were finely pulverized and thoroughly mixed, and then the mixture was loaded into a Carius tube. The tube was sealed under a vacuum and placed into a preheated oven maintained at desired temperatures. During the reaction, the progress could be visually monitored by a gradual color change. After the reaction was completed, the tube was opened, and the contents were extracted with a minimal amount of CH₂Cl₂; the solution was then subjected to column chromatography resulting in the isolation of pure Os products. This solid-state pyrolysis technique appears to be very simple and has the advantage of allowing us to conduct the reactions at higher temperatures free from the interference of organic solvents.²¹ In contrast, the second-row analogues, such as [Ru(bpy)(CO)₂Cl₂], were prepared from [Ru(CO)₃Cl₂]₂ or the oligomeric reagent [Ru(CO)₂Cl₂]_n with a diimine ligand, such as 2,2'-bipyridine (bpy), in refluxing alcohol or THF solutions.²² The success of this approach is apparently the result of the much higher reactivity of the Ru reagents.

The isolated products were then analyzed by routine spectroscopic methods. The EI MS analysis of all of the samples exhibited the anticipated molecular ion (M⁺) with *m/z* values equal to the molecular mass of diimine ligand plus that of the Os(CO)₂I₂ unit. ¹³C NMR analyses of complexes **1–3** showed only one signal in the δ 178.0–178.4 region with an intensity corresponding to two CO ligands, along with the signals derived from the diimine ligands. In addition, IR analyses of all of the complexes in solution gave two intense ν(CO) stretching bands of equal intensity, implying that the CO ligands could reside at the cis disposition. It is also notable that the ν(CO) signals of

- (20) Chan, L.-H.; Lee, R.-H.; Hsieh, C.-F.; Yeh, H.-C.; Chen, C.-T. *J. Am. Chem. Soc.* **2002**, *124*, 6469.
- (21) (a) Gong, J.-H.; Hwang, D.-K.; Tsay, C.-W.; Chi, Y.; Peng, S.-M.; Lee, G.-H. *Organometallics* **1994**, *13*, 1720. (b) Gong, J.-H.; Chen, C.-C.; Chi, Y.; Wang, S.-L.; Liao, F.-L. *J. Chem. Soc., Dalton Trans.* **1993**, 1829.
- (22) (a) Chardon-Noblat, S.; Deronzier, A.; Ziessel, R.; Zsoldos, D. *Inorg. Chem.* **1997**, *36*, 5384. (b) Homanen, P.; Haukka, M.; Luukkanen, S.; Ahlgren, M.; Pakkanen, T. A. *Eur. J. Inorg. Chem.* **1999**, 101.

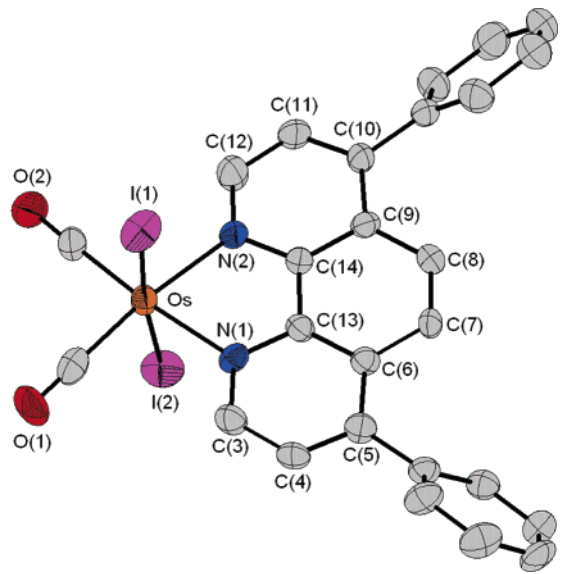


Figure 1. ORTEP diagram of complex **3** with thermal ellipsoids shown at the 50% probability level.

pboz complex **4** (2041 and 1978 cm^{-1}) occurred at a higher energy level than those of the bpy and dpphen complexes: cf. **1** (2038 and 1974 cm^{-1}) and **3** (2037 and 1973 cm^{-1}). This trend indicates that the pboz ligand has a better π -acceptor strength because of the presence of an extra oxygen atom, which reduces the electron density on the Os atom and decreases the degree of back π -bonding to CO ligands. In contrast, the addition of *tert*-butyl substituents to the chelating bipyridine ligand of **1** caused a slight decrease in the CO stretching energies, the result of which is consistent with its better electron-donating characteristics, as indicated by the IR $\nu(\text{CO})$ stretching frequencies of **2**.

Further confirmation of the proposed molecular structures is provided by single-crystal X-ray analysis of the dpphen complex **3**. Its ORTEP diagram is displayed in Figure 1, and the bond distances and angles are listed in Table 2. It is pertinent to note that the Os atom showed a slightly distorted octahedral ligand arrangement. Both CO ligands are located opposite of the N atoms of the chelating dpphen ligand with the Os–N distances ($\text{Os}–\text{N}(1) = 2.113(7)$ Å and $\text{Os}–\text{N}(2) = 2.115(7)$ Å) being slightly longer than those observed in the cationic Os(II) complexes, such as $[\text{Os}(\text{bpy})_3][\text{PF}_6]_2$ and $[\text{Os}(\text{bpy})_2(\text{Cl})(\text{NCMe})][\text{PF}_6]$ (2.036–2.076 Å),²³ while its phenyl substituents are twisted against the phenanthroline unit to reduce the steric congestion. Two iodides are located at the mutual trans position and lean slightly toward the dpphen ligand with $\angle \text{I}(1)–\text{Os}–\text{I}(2) = 173.93(3)^\circ$; this may be the result of the crystal packing effect. The Os–I distances ($\text{Os}–\text{I}(1) = 2.7002(7)$ Å and $\text{Os}–\text{I}(2) = 2.6781(7)$ Å) are shorter than those of the structurally characterized complex $[\text{Os}(\text{dbm})(\text{CO})_3\text{I}]$ (2.721(1) Å),²⁴ in which the unique iodine ligand is trans to a much stronger π -accepting carbonyl ligand. Finally, the overall ligand arrangement of **3** is related

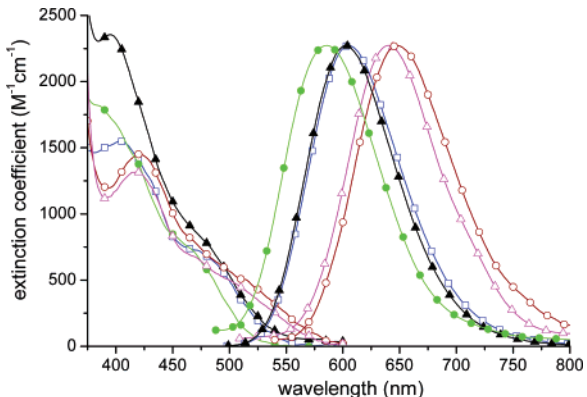


Figure 2. UV–vis absorption and emission spectra of **1** (blue squares), **2** (green circles), **3** (black triangles), **4** (red circles), and **5** (magenta triangles) in CH_2Cl_2 at room temperature. The emission spectra were acquired under degassed condition.

to that of the Ru analogues, $[\text{Ru}(\text{bpy})(\text{CO})_2\text{Cl}_2]$ and $[\text{Ru}(\text{dmbpy})(\text{CO})_2\text{Cl}_2]$,²⁵ showing thermodynamically more stable trans (halide, halide) and cis (CO, CO) configurations.

Photophysical Properties. The UV–vis spectra of these complexes are depicted in Figure 2. In all cases, the spectra are characterized by an intense ligand-localized $\pi–\pi^*$ transition in the UV region, accompanied by a broad moderately intense band which extends beyond 470 nm; this band can be plausibly attributed, by its analogy to similar Re(I) and Ru(II) diimine carbonyl complexes that were reported in the literature,²⁶ to an MLCT transition mixed, in part, with an XLCT transition. It should also be noted that given the strong spin–orbit coupling in Os(II) complexes, both singlet and triplet absorption bands could be present. Further firm support of this assignment will be elaborated in the Theoretical Approaches section (vide infra). In general, the differentiation of XLCT from MLCT can be attributed to certain extents of mixing between the metal d_π and halide p_π orbitals, resulting in two sets of orbitals with metal–halide bonding and antibonding characteristics. In the case of the iodide complexes, the energy of the iodide p_π orbitals is comparable to that of the metal d_π orbitals. Thus, mixing between the p_π and d_π orbitals is expected; the net result of this mixing is an increase of the iodide character in the HOMO of the metal complexes. Consequently, the lowest-energy excited state may originate from a transition incorporating the $d_\pi(\text{Os})–p_\pi(\text{I})$ antibonding orbital and the π^* orbital of the chelating ligand.

In good agreement with the MLCT/XLCT assignment, the intensity of the lowest-energy transition is notably smaller than that of the typical MLCT transition because of the poor orbital overlap and, hence, the transition dipole between the iodide p_π and the ligand π^* orbitals. Accordingly, as shown in Figure 2, the corresponding peak wavelength can only be vaguely determined because of its strong spectral overlaps with the higher energy, much more intense, ligand-centered $\pi\pi^*$ absorptions. Moreover, in the case of dpphen complex

(23) (a) Constable, E. C.; Raithy, P. R.; Smit, D. N. *Polyhedron* **1989**, *8*, 367. (b) Demadis, K. D.; Meyer, T. J.; White, P. S. *Inorg. Chem.* **1998**, *37*, 3610.

(24) Chen, Y.-L.; Sinha, C.; Chen, I.-C.; Liu, K.-L.; Chi, Y.; Yu, J.-K.; Chou, P.-T.; Lu, T.-H. *Chem. Commun.* **2003**, 3046.

(25) (a) Haukka, M.; Kiviaho, J.; Ahlgren, M.; Pakkanen, T. A. *Organometallics* **1995**, *14*, 825. (b) Homanen, P.; Haukka, M.; Pakkanen, T. A.; Pursiainen, J.; Laitinen, R. H. *Organometallics* **1996**, *15*, 4081.

(26) Stufkens, D. J.; Arnts, M. P.; Rossenaar, B. D.; Vleek, A., Jr. *Pure Appl. Chem.* **1997**, *69*, 831.

Table 3. Photophysical and Electrochemical Properties of Os Complexes **1–5** in CH₂Cl₂ at Room Temperature

	abs λ_{max} (nm) [ϵ (M ⁻¹ cm ⁻¹)]	PL λ_{max} (nm) ^a	$\Phi_{\text{degassed}}^{\text{a}}$	τ (ns) ^a	$E_{1/2}^{\text{ox}} (\Delta E_p)^c$	$E_{1/2}^{\text{red}} d$
1	283, 296, 350, 404, 480 (21327, 21858, 2434, 1550, 682)	606 (533)	0.15 (−) ^b	239 (18)	0.86 (95)	−1.94
2	284, 350, 390, 466 (24166, 2466, 1785, 737)	583 (537)	0.02 (−) ^b	25 (32)	0.86 (105)	−2.01
3	287, 327, 395, 474 (30532, 8325, 2355, 831)	604 (576)	0.39 (0.25)	556 (200)	0.86 (90)	−1.81
4	280, 325, 421, 470 (sh), 500 (18601, 19353, 1451, 784, 567)	650 (600)	0.02 (0.12)	295 (254)	0.92 (100)	−1.62
5	280, 338, 354, 418, 502 (16320, 20984, 15036, 1317, 492)	640 (597)	0.02 (0.08)	83 (598)	0.92 (95)	−1.67

^a Data in parentheses show the data measured in a solid film. The solid film was prepared using vacuum deposition. ^b The intensity was weak; therefore the quantum yield determined in the solid film is not reliable and hence is not listed here. ^c Oxidation potentials are measured in a 0.1 M solution of (NBu₄)PF₆ in CH₂Cl₂ and reported in volts using Fc/Fc⁺ as a reference, which is equivalent to 0.23 V vs the Ag/AgNO₃ reference potential. $\Delta E_p = E_{\text{ap}}$ (anodic peak potential) − E_{cp} (cathodic peak potential), and the data are quoted in millivolts. ^d All irreversible cathodic potentials are measured in a 0.1 M solution of (NBu₄)PF₆ in THF and reported in volts using Fc/Fc⁺ as a reference, which is equivalent to 0.18 V vs the Ag/AgNO₃ reference potential.

3, a greatly enhanced extinction coefficient has been observed with respect to those of **1** and **2**. This is likely to be the result of the additional extended π -delocalization provided by the ancillary phenyl substituents on phenanthroline. It is also notable that the absorption of the second class of pboz complexes, **4** and **5**, exhibits a substantial bathochromatic shift in comparison to those of the more symmetrical complexes, **1–3**. We speculate that the electronegative oxygen atom of benzoxazole not only causes the breakdown of the overall molecular symmetry but also manipulates the π^* orbital of the pboz ligand to lower the relative orbital energy, resulting in an increase in the extinction coefficient for the $\pi-\pi^*$ transition as well as a substantial reduction of the MLCT/XLCT transition energies.

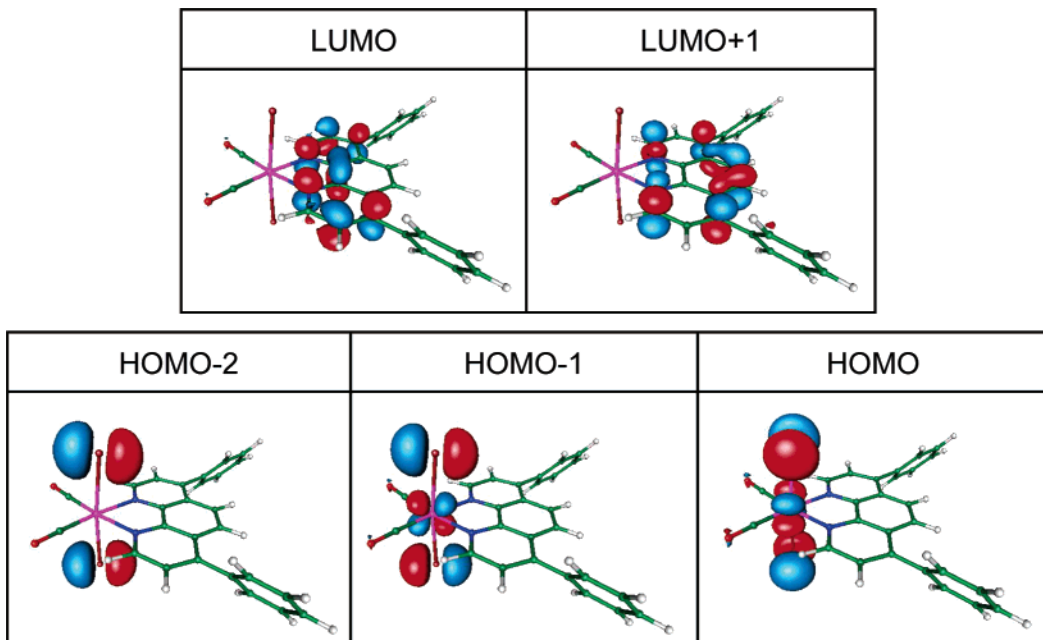
Moderate to strong emissions were observed for **1–5** both in solution and as a solid film at room temperature. The corresponding data are outlined in Table 3, while the spectra recorded in a deoxygenated CH₂Cl₂ solution are depicted in Figure 2. In each complex, the entire emission band, originating from a common ground-state species, is ascertained by the same emission excitation spectra throughout the monitored wavelengths of 500–750 nm (not shown here). Furthermore, the excitation spectra, within experimental error, are also effectively identical to the absorption spectrum which indicates that the entire phosphorescence results from a common Franck–Condon excited state. In all cases, both a large Stokes shift and a structureless peak profile are suggestive of an emission originating from the triplet manifold, possibly possessing the aforementioned MLCT/XLCT character, which is populated from rapid intersystem crossing as a result of a large spin–orbit coupling. The emission maxima, λ_{max} , for complexes **1**, **2**, and **3** occurred at 606, 583, and 604 nm, respectively, in CH₂Cl₂ at room temperature revealing a good correlation with respect to the energetics of the lowest-energy absorption band elaborated previously; namely, the substitution of a dbubpy ligand for the bpy and dpphen ligands leads to a notable blue shift of the emission peak wavelength in complex **2**.

Moreover, replacing the bpy ligand with the pboz ligand leads to a significant bathochromic shift of the emission. The result implies that the benzoxazole ligand of **4** and **5** possesses a lower-energy π^* orbital relative to that of the bpy ligands, which in turn results in a large reduction of the

energy gap for the MLCT/XLCT excited states, in accordance with the trend resolved from the absorption spectra. Finally, both the emission lifetimes and the quantum yields of the *tert*-butyl-substituted complexes, **2** and **5**, were relatively smaller than those of their parent complexes, **1** and **4**, respectively. These observations may be rationalized by the excessive internal motions introduced by the *tert*-butyl substituent which provide an efficient radiationless pathway back to the ground state.

Electrochemistry. Cyclic voltammetric data were recorded in CH₂Cl₂ and THF solutions involving 0.1 M (NBu₄)PF₆ at a scan rate of 100 mV/s. The corresponding redox potentials are presented in Table 3. For **1–5**, the results showed a reversible metal-centered oxidation process and ligand-based irreversible reduction peaks. It is notable that benzoxazole complexes **4** and **5** exhibit significantly lower oxidation and reduction potentials compared to those of the bipyridine and phenanthroline complexes, **1–3**. Apparently, the electronegative oxygen atom in the benzoxazole ligand decreases its ability to donate electrons to the central Os(II) d_π orbitals and also lowers the relative energy of the ligand-based π^* molecular orbital. This electron-withdrawing effect correlates well with the observed trend in electrochemical potentials.

Theoretical Approaches. Theoretical confirmation of the underlying basis for the photophysical properties of these osmium complexes was provided by the ab initio MO calculations. The results for complex **3** are shown in Figure 3 and Table 4. Figure 3 depicts the features of the two lowest-unoccupied (LUMO and LUMO+1) and the three highest-occupied (HOMO, HOMO-1, and HOMO-2) frontier orbitals, mainly involved in the lower-lying transition, while the descriptions and the energy gap of each transition are listed in Table 4. Apparently, the electron densities of the singlet and triplet states for both the HOMO and HOMO-1 are located largely on the central metal and iodide atoms, whereas those of the LUMO are mainly distributed on the phenanthroline moiety; this indicates that the lowest electronic transition is dominated by MLCT/XLCT character. The lowest triplet state calculated for **3** is in good agreement with that obtained experimentally (643 and 604 nm, respectively). The small energy gap between the calculated T₁–S₀ (643 nm) and S₁–S₀ (628 nm) energy gaps seems reasonable because of the strong spin–orbit coupling and hence the

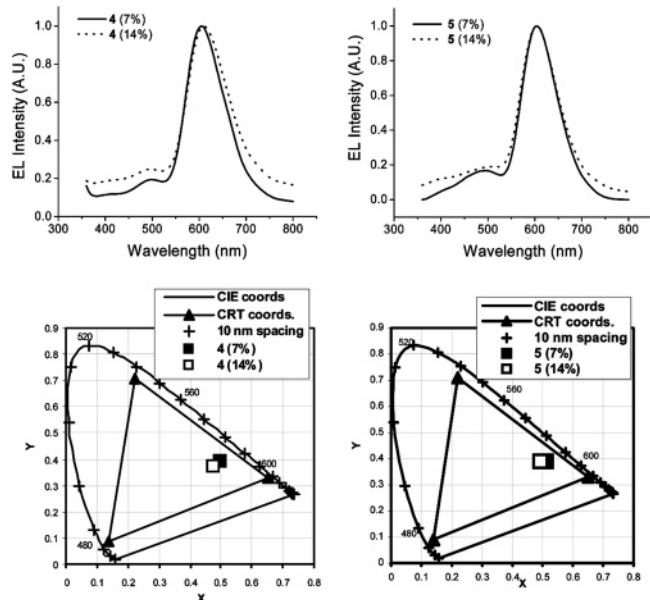
**Figure 3.** Selected frontier orbitals of complex **3**.**Table 4.** Calculated Energy Levels of the Lowest Four Transitions of Complex **3**

λ (nm)	E (eV)	ϕ	assignment	character (%) ^a
T ₁	643.9	1.93	\sim 0	HOMO \rightarrow LUMO
T ₂	633.4	1.96	\sim 0	HOMO-1 \rightarrow LUMO
S ₁	628.8	1.97	0.001	HOMO \rightarrow LUMO
S ₂	604.4	2.05	0.0159	HOMO-1 \rightarrow LUMO
S ₃	569.8	2.18	0.0131	HOMO \rightarrow LUMO+1
S ₄	562.2	2.21	0.0062	HOMO-1 \rightarrow LUMO+1
S ₅	480.5	2.58	0.0001	HOMO-2 \rightarrow LUMO

^a This percentage was estimated from the contribution of the iodine orbital in HOMO (or HOMO-1). Note that LUMO is solely located at the dpphen ligand. The rest of the percentage is mainly attributed to MLCT.

mixing between singlet and triplet manifolds. The deviation of the current theoretical approach from the experimental results may plausibly be explained by the underestimation of the mixing of high-density low-lying states or the less-extensive basis set used for the iodide atoms. Nevertheless, the result qualitatively predicts the tendencies of the relative energy levels of these lower-lying excited states. Similar results were obtained for other complexes, in which the lower-lying transitions all possess mixing XLCT/MLCT character. The results are not elaborated in detail here to avoid redundancy. Obviously, the theoretical level adopted here is suitable for studying the photophysical properties of the complexes concerned in a qualitative manner.

Electroluminescence. Considering the most bathochromic shifting of the emission wavelength beyond 600 nm, electroluminescent devices using pboz complexes **4** and **5** as the dopant emitters (in two concentrations of 7% and 14%) were fabricated for the possible red phosphorescent OLEDs. Our devices have the conventional multilayer configuration ITO/NPB (40 nm)/CBP (30 nm)/**4** or **5** (7% and 14%)/BCP (10 nm)/AlQ₃ (30 nm)/MgAg where NPB (1,4-bis(1-naphthyl phenylamino)biphenyl) serves as the hole transporting layer and CBP (4,4'-bis(9-carbazolyl)biphenyl), BCP (2,9-di-methyl-4,7-diphenyl-1,10-phenanthro line), and AlQ₃ (tris-

**Figure 4.** Electroluminescence spectra and the corresponding 1931 CIE chromaticity diagram of OLEDs containing dopant **4** or **5** with 7% and 14% doping concentrations.

(8-hydroxyquinolinyl)aluminum) function as the host matrix for the orange-red emitting **4** and **5**, hole blocking layer, and electron transporting layer, respectively. All devices exhibit electroluminescence (EL) centered around 600–610 nm (Figure 4), which corresponds well to the orange-red photoluminescence (PL) of the pboz complexes in solution. However, a couple of weak emission signals with shorter wavelengths around 370–520 nm were also clearly observed for all of the OLED devices. While the short wavelength EL in the region of 370–420 nm can be attributed to the fluorescence of host matrix CBP,²⁷ the origin of the EL with

(27) Adamovich, V.; Brooks, J.; Tamayo, A.; Alexander, A. M.; Djurovich, P.; D'Andrade, B. W.; Adachi, C.; Forrest, S. R.; Thompson, M. E. *New J. Chem.* **2002**, 26, 1171.

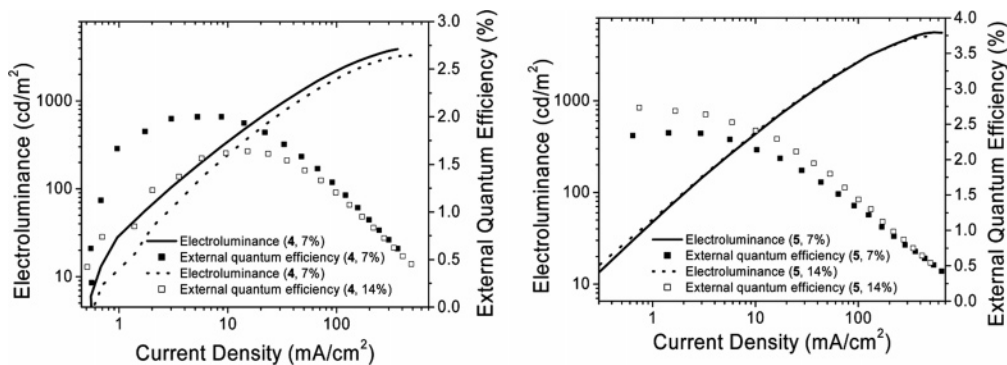


Figure 5. Electroluminescence external quantum efficiency current density characteristics of OLEDs containing dopant **4** or **5** with 7% and 14% doping concentrations.

λ_{\max} around 500 nm is not readily known. These short wavelength emissions, to a certain extent, perturb the red emission of Os(II) complexes, and consequently, all of these devices exhibited orange emissions instead of red emissions as indicated by the 1931 CIE color chromaticity of 0.48–0.50 and 0.37–0.39, and 0.49–0.51 and 0.39, for OLEDs based on **4** and **5**, respectively (Figure 4). The orange device can be as bright as 5600 cd/m^2 (OLED containing dopant **5** in a 7% doping level) (Figure 5). The highest EL efficiency is 2.8% (5.0 cd/A or 2.7 lm/W) for the external quantum efficiency observed for the OLED with a 14% dopant concentration of **5** at a low current density of less than 0.5 mA/cm^2 (at a driving voltage of ~ 7.5 V) (Figure 5). With a 15 V driving voltage, all of the devices showed rather high current resistances and relatively low current densities in the range of 350–650 mA/cm^2 (Figure 5). These high current resistances are probably the result of the strong charge trapping properties for the carbonyl ligands associated with Os(II) complex **4** or **5**. Finally, note that an additional emission band centered around 456 nm was observed for the nondopant device with configuration ITO/NPB (40 nm)/**4** (30 nm)/BCP (10 nm)/AlQ₃ (30 nm)/MgAg. We tentatively attribute this 456 nm emission band to the fluorescence from the NPB and BCP layers, the result of which may qualitatively rationalize the origin of the weak 500 nm emission observed for the dopant devices. In comparison, the efficiencies and color purity of the devices are inferior to those of the recently reported osmium-based red emitting complexes,²⁸ for which all of the carbonyl ligands were removed to improve the associated photophysical properties and thermal stability.

4. Conclusion

In conclusion, we have synthesized and characterized a new series of Os(II) diimine complexes. Both photophysical

and theoretical approaches lead us to conclude that the lowest singlet and triplet transitions are associated with a large amount of XLCT character. The feasibility of OLED performance, in turn, has been demonstrated using complexes **4** and **5**. The interplay between XLCT and MLCT should be of great fundamental interest. For instance, the mixing ratio for XLCT versus MLCT can be fine-tuned by another nonhalide axial ligand via its electron-donating/electron-withdrawing properties.^{7,26} One thus expects that as the XLCT character increases, the change of dipolar vector between the ground and excited (triplet) states should increase because of the interligand electronic transition. The large dipolar changes in the solute are normally coupled with the solvent polarity coordinate. Upon excitation, the alternation of the equilibrium polarization should result in remarkable phosphorescence solvatochromism in solution. As a result, a wide range of color tunability can be achieved, which may spark broad interest in the relatively new field of the solvation dynamics of phosphorescence²⁹ as well as in the search for color tuning for application.

Acknowledgment. This work was funded by the National Science Council of Taiwan, ROC (Grants NSC 91-2119-M-002-016 and NSC 91-2113-M-007-006). Y.C. thanks Dr. C. Sinha for his initial assistance with experiments.

Supporting Information Available: X-ray crystallographic data file for complex **3** and additional crystal data and structure refinements, atomic coordinates and displacement parameters, bond lengths and angles, anisotropic displacement parameters, and hydrogen coordinates and isotropic displacement parameters for complex **3**. This material is available free of charge via the Internet at <http://pubs.acs.org>.

IC050036Y

(28) (a) Tung, Y.-L.; Lee, S.-W.; Chi, Y.; Tao, Y.-T.; Chien, C.-H.; Cheng, Y.-M.; Chou, P.-T.; Peng, S.-M.; Liu, C.-S. *J. Mater. Chem.* **2005**, *15*, 460. (b) Tung, Y.-L.; Wu, P.-C.; Liu, C.-S.; Chi, Y.; Yu, J.-K.; Hu, Y.-H.; Chou, P.-T.; Peng, S.-M.; Lee, G.-H.; Tao, Y.; Carty, A. J.; Shu, C.-F.; Wu, F.-I. *Organometallics* **2004**, *23*, 3745.

(29) Yu, J.-K.; Cheng, Y.-M.; Hu, Y.-H.; Chou, P.-T.; Chen, Y.-L.; Lee, S.-W.; Chi, Y. *J. Phys. Chem. B* **2004**, *108*, 19908.